Development of a 3D non-hydrostatic pressure model for free surface flows

J. W. Lee* M. D. Teubner† J. B. Nixon‡ P. M. Gill§

(Received 8 October 2004, revised 7 June 2005)

Abstract

A three-dimensional, non-hydrostatic pressure, numerical model for free surface flows is presented. By decomposing the pressure term into hydrostatic and non-hydrostatic parts, the numerical model uses an integrated time step with two fractional steps. In the first fractional step, the momentum equations are solved without the hydrostatic pressure term using Newton's method in conjunction with the generalised minimal residual (GMRES) method. This combined method does not require the determination of a Jacobian matrix explicitly but simply the product of the Jacobian and a vector, thereby reducing the amount of storage required and significantly decreasing the overall

*Applied Mathematics, The University of Adelaide, South Australia, AUSTRALIA. mailto:jong.lee@adelaide.edu.au

†Applied Mathematics, The University of Adelaide, South Australia, AUSTRALIA.

‡United Water International, GPO Box 1875, South Australia, AUSTRALIA.

§Applied Mathematics, The University of Adelaide, South Australia, AUSTRALIA.

See http://anziamj.austms.org.au/V46/CTAC2004/Lee1 for this article, Published July 12, 2005. ISSN 1446-8735

computational time required. By using Newton's method, the numerical model can handle implicitly almost all variables, unlike many other numerical models. Hence numerical stability is achieved effectively. In the second fractional step, the pressure-Poisson equation is solved iteratively with a preconditioned linear GMRES method. It is shown that preconditioning reduces the processing time dramatically. After the new pressure field is obtained the intermediate velocities, which are calculated from the previous fractional step, are updated and then these updated velocities preserve the local mass conservation. The newly developed model is verified against analytical solutions, with good agreement.

Contents

1 Introduction

Over the past two decades, three-dimensional (3D) models have been extensively developed and used with the hydrostatic pressure approximation [5, 7]. If the hydrostatic pressure approximation is assumed, the vertical momentum

equation is omitted and the vertical velocity is calculated from the continuity equation. Numerical models that use this approximation are applied to many shallow water flows. However, in some flows in which the ratio of the wave length to the depth is small, this approximation is inaccurate. More recently, as computer power has increased dramatically, a few numerical models have been developed that determine the non-hydrostatic pressure by solving a pressure-Poisson equation [2, 6, 10]. The numerical techniques for the pressure-Poisson equation are usually either the semi-implicit method for the pressure-linked equation (SIMPLE)-family methods [8] or fractional time step methods [6]. The SIMPLE methods need multiple iterations per time step until the pressure has converged. Alternatively a fractional time step method is employed by separating the pressure term into hydrostatic and non-hydrostatic parts and using time marching computations.

In other non-hydrostatic models [2, 6], only parts of the equations are treated implicitly and then the resulting matrix inverted inexpensively. For example, the water surface elevation and the vertical diffusion terms in the momentum equations are discretised implicitly in Casulli [2]. In this way, the velocity field is obtained by inverting a tri-diagonal matrix after the water surface elevation is determined. In this study, most terms are solved implicitly using Newton's method with an almost matrix-free methodology. For maximum flexibility in the representation of the computational domain, the governing equations are solved in a generalised coordinate system.

2 Mathematical formulation

In many hydrostatic models [5, 7], it is assumed that the pressure variations depend on the amount of water above a point in vertical space so that it is a function of water surface elevation only, leading to the hydrostatic approximation. However, in this model, the pressure is decomposed into hydrostatic

and non-hydrostatic (or hydrodynamic) parts [2]:

$$P = \rho g\,(h - z) + q\,, \tag{1}$$

where $q(x, y, z, t)$ is the non-hydrostatic pressure.

In order to be able to apply this model to irregular boundary and free surface problems, the inviscid 3D Navier–Stokes equations are transformed from the Cartesian coordinate system (x, y, z, t) to a generalised coordinate system (ξ, η, ζ, τ) [4]. With the pressure decomposition, the transformed Navier–Stokes equations are

$$\frac{\partial}{\partial \xi}\left(\frac{U}{J}\right) + \frac{\partial}{\partial \eta}\left(\frac{V}{J}\right) + \frac{\partial}{\partial \zeta}\left(\frac{W}{J}\right) = 0\,, \tag{2}$$

$$\frac{\partial \mathbf{Q}}{\partial \tau} + \frac{\partial \mathbf{E}}{\partial \xi} + \frac{\partial \mathbf{F}}{\partial \eta} + \frac{\partial \mathbf{G}}{\partial \zeta} = \mathbf{P_h} + \mathbf{P_d}\,, \tag{3}$$

where: $\mathbf{Q}$ represents the unknown variables; $\mathbf{E}$, $\mathbf{F}$ and $\mathbf{G}$ are inviscid fluxes in the ξ, η and ζ directions, respectively; $\mathbf{P_h}$ and $\mathbf{P_d}$ represent the hydrostatic and non-hydrostatic pressure terms, respectively; and the Jacobian of the transformation

$$J = 1/[x_\xi(y_\eta z_\zeta - y_\zeta z_\eta) - x_\eta(y_\xi z_\zeta - y_\zeta z_\xi) + x_\zeta(y_\xi z_\eta - y_\eta z_\xi)]\,. \tag{4}$$

In matrix form, we define

$$\mathbf{Q} = \frac{1}{J}\begin{pmatrix} u \\ v \\ w \end{pmatrix}, \quad \mathbf{E} = \frac{U}{J}\begin{pmatrix} u \\ v \\ w \end{pmatrix}, \quad \mathbf{F} = \frac{V}{J}\begin{pmatrix} u \\ v \\ w \end{pmatrix}, \quad \mathbf{G} = \frac{W + \zeta_t}{J}\begin{pmatrix} u \\ v \\ w \end{pmatrix}, \tag{5}$$

$$\mathbf{P_h} = -g\begin{pmatrix} \left(\frac{\xi_x}{J}H\right)_\xi + \left(\frac{\eta_x}{J}H\right)_\eta + \left(\frac{\zeta_x}{J}H\right)_\zeta \\ \left(\frac{\xi_y}{J}H\right)_\xi + \left(\frac{\eta_y}{J}H\right)_\eta + \left(\frac{\zeta_y}{J}H\right)_\zeta \\ 0 \end{pmatrix}, \tag{6}$$

$$\mathbf{P_d} = -\frac{1}{\rho}\begin{pmatrix} \left(\frac{\xi_x}{J}q\right)_\xi + \left(\frac{\eta_x}{J}q\right)_\eta + \left(\frac{\zeta_x}{J}q\right)_\zeta \\ \left(\frac{\xi_y}{J}q\right)_\xi + \left(\frac{\eta_y}{J}q\right)_\eta + \left(\frac{\zeta_y}{J}q\right)_\zeta \\ \left(\frac{\xi_z}{J}q\right)_\xi + \left(\frac{\eta_z}{J}q\right)_\eta + \left(\frac{\zeta_z}{J}q\right)_\zeta \end{pmatrix}, \tag{7}$$

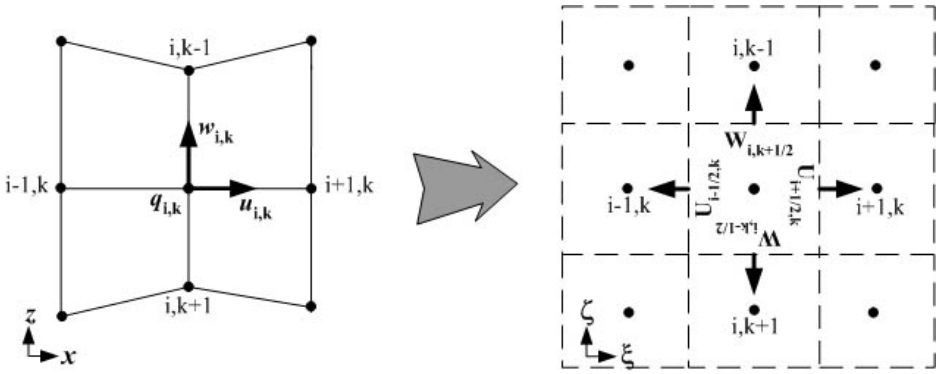

FIGURE 1: Grid transformation and normal velocities at the cell faces

where H is the water surface elevation. The normal velocities at the cell faces (Figure 1) are and are determined by

$$\begin{aligned} U &= \xi_x u + \xi_y v + \xi_z w \,, \\ V &= \eta_x u + \eta_y v + \eta_z w \,, \\ W &= \zeta_x u + \zeta_y v + \zeta_z w \,. \end{aligned} \tag{8}$$

In Figure 1, all variables except the normal velocities are defined at the cell centre, resulting in a staggered grid scheme. In collocated grids, a checker board pressure field [8] may occur. However, this is prevented by locating the normal velocities at the cell faces.

For the free surface, integrate the incompressible Cartesian form of the continuity equation from the bottom to the surface and then transform to the generalised coordinate system leading to

$$\frac{\partial}{\partial \tau}\left(\frac{h}{J}\right) + \frac{\partial}{\partial \xi}\left(\frac{h\bar{U}}{J}\right) + \frac{\partial}{\partial \eta}\left(\frac{h\bar{V}}{J}\right) = 0 \,, \tag{9}$$

where: $\bar{U} = \left[\xi_x \int_{z_b}^{H} u\, dz + \xi_y \int_{z_b}^{H} v\, dz\right] / h$; $\bar{V} = \left[\eta_x \int_{z_b}^{H} u\, dz + \eta_y \int_{z_b}^{H} v\, dz\right] / h$; h is the water depth; and z_b is the bottom elevation.

3 Numerical approximation

For the numerical approximation of the inviscid fluxes, the symmetric total variation diminishing (TVD) method [11] is used, wherein rapid changes in the flow fields are captured using a three-point stencil in one direction. We define the numerical fluxes at cell faces as

$$\mathbf{E}^*_{i+1/2,j,k} = \frac{1}{2}\left(\mathbf{E}_{i,j,k} + \mathbf{E}_{i+1,j,k}\right) - \frac{1}{2}U_{i+1/2,j,k}(1-\phi_{i+1/2,j,k})\Delta\mathbf{Q}_{i+1/2,j,k}\,, \quad (10)$$

where $\Delta\mathbf{Q}_{i+1/2,j,k} = \mathbf{Q}_{i+1,j,k} - \mathbf{Q}_{i,j,k}$, and

$$\phi_{i+1/2,j,k} = \text{minmod}(1, r^+) + \text{minmod}(1, r^-) - 1\,, \quad (11)$$

where:

$$r^+ = \frac{\mathbf{Q}_{i-1/2,j,k}}{\mathbf{Q}_{i+1/2,j,k}}\,; \quad \text{and} \quad r^- = \frac{\mathbf{Q}_{i+3/2,j,k}}{\mathbf{Q}_{i+1/2,j,k}}\,; \quad (12)$$

and the minmod function is defined as

$$\text{minmod}(x,y) = \begin{cases} 0 & \text{for } xy \le 0\,, \\ x & \text{for } |x| \le |y|\,, \\ y & \text{for } |x| > |y|\,. \end{cases} \quad (13)$$

Linear interpolation is used to find U at cell faces. A similar approximation is applied for the η and ζ directional fluxes and the depth integrated fluxes in the water surface equation.

For time integration, the equations (2)–(9) are solved using two fractional time steps. For the first (hydrostatic pressure) step, equation (3) without the non-hydrostatic term is

$$\mathcal{F}(\tilde{\mathbf{Q}}) = \frac{\partial\tilde{\mathbf{Q}}}{\partial\tau} + \frac{\partial\tilde{\mathbf{E}}}{\partial\xi} + \frac{\partial\tilde{\mathbf{F}}}{\partial\eta} + \frac{\partial\tilde{\mathbf{G}}}{\partial\zeta} - \tilde{\mathbf{P}}_\mathbf{d} = 0\,, \quad (14)$$

where: $\mathcal{F}$ is the function representing the momentum equations to be solved; and $\tilde{\mathbf{Q}}$, etc. denote intermediate solutions which are to be modified in the

second step by solving for the non-hydrostatic pressure. This equation is solved using the Newton–GMRES method with a matrix-free technique [1].

In the second (non-hydrostatic pressure) step, the new velocities are calculated by considering the non-hydrostatic pressure term so that the velocities satisfy local mass conservation. Write the non-hydrostatic pressure with the time derivatives of velocities in semi-discrete form as

$$\begin{aligned}
\frac{u^{n+1}}{J} &= \frac{\tilde{u}}{J} - \frac{\Delta\tau}{\rho}\left[\left(\frac{\xi_x}{J}q\right)_\xi + \left(\frac{\eta_x}{J}q\right)_\eta + \left(\frac{\zeta_x}{J}q\right)_\zeta\right], \\
\frac{v^{n+1}}{J} &= \frac{\tilde{v}}{J} - \frac{\Delta\tau}{\rho}\left[\left(\frac{\xi_y}{J}q\right)_\xi + \left(\frac{\eta_y}{J}q\right)_\eta + \left(\frac{\zeta_y}{J}q\right)_\zeta\right], \\
\frac{w^{n+1}}{J} &= \frac{\tilde{w}}{J} - \frac{\Delta\tau}{\rho}\left[\left(\frac{\xi_z}{J}q\right)_\xi + \left(\frac{\eta_z}{J}q\right)_\eta + \left(\frac{\zeta_z}{J}q\right)_\zeta\right].
\end{aligned} \tag{15}$$

Substituting equation (15) into equation (2) gives an elliptic equation, which is called the pressure-Poisson equation. After approximating the second order derivatives of the Poisson equation using

$$\begin{aligned}
\frac{\partial}{\partial\xi}\left(L\frac{\partial M}{\partial\xi}\right) &= \frac{1}{(\Delta\xi)^2}[L_{i+1/2,j,k}(M_{i+1,j,k} - M_{i,j,k}) \\
&\qquad - L_{i-1/2,j,k}(M_{i,j,k} - M_{i-1,j,k})]\,,
\end{aligned} \tag{16a}$$

$$\begin{aligned}
\frac{\partial}{\partial\xi}\left(L\frac{\partial M}{\partial\eta}\right) &= \frac{1}{4\Delta\xi\Delta\eta}[L_{i+1/2,j,k}(M_{i+1,j+1,k} - M_{i+1,j-1,k} \\
&\qquad + M_{i,j+1,k} - M_{i,j-1,k}) \\
&\qquad - L_{i-1/2,j,k}(M_{i,j+1,k} - M_{i,j-1,k} \\
&\qquad + M_{i-1,j+1,k} - M_{i-1,j-1,k})]\,,
\end{aligned} \tag{16b}$$

a heavily banded matrix is obtained; this is inverted using a preconditioned linear GMRES method.

This preconditioning has been performed using the equation

$$\mathbf{A}\mathbf{M}^{-1}\mathbf{x}^* = \mathbf{b} \quad \text{with} \quad \mathbf{x}^* = \mathbf{M}\mathbf{x}\,, \tag{17}$$

where: $\mathbf{A}$ is the coefficient matrix; $\mathbf{M}$ is the preconditioner; $\mathbf{x}^*$ is the unknown vector to be solved; $\mathbf{b}$ is the known vector; and $\mathbf{x}$ is the solution containing the non-hydrostatic pressure. When the coefficient matrix is expressed as the sum of diagonal ($\hat{\mathbf{D}}$), strictly lower ($\hat{\mathbf{E}}$), and strictly upper ($\hat{\mathbf{F}}$) matrices, it is factorised as

$$\mathbf{A} = \hat{\mathbf{E}} + \hat{\mathbf{D}} + \hat{\mathbf{F}} = (\hat{\mathbf{E}}\hat{\mathbf{D}}^{-1} + \mathbf{I})(\hat{\mathbf{D}} + \hat{\mathbf{F}}) - \boldsymbol{\mathcal{E}} = \mathbf{LU} - \boldsymbol{\mathcal{E}}\,, \tag{18}$$

where $\boldsymbol{\mathcal{E}} = \hat{\mathbf{E}}\hat{\mathbf{D}}^{-1}\hat{\mathbf{F}}$ is the error in the above factorisation and $\mathbf{L}$ and $\mathbf{U}$ are, respectively, lower and upper triangular matrices that are determined easily by backward and forward substitution. If the $\mathbf{LU}$ matrix is used as a preconditioner—the symmetric Gauss–Seidel (SGS) method [9]—the factorisation error is ignored.

In the current grid system, dynamic pressure boundary conditions are replaced by specifying a normal velocity. For instance, $U_{-1/2,j,k} = U_{1/2,j,k}$ are applied to an impermeable boundary wall ($i = 1$). When the new pressure field is obtained, velocities are updated using equation (15) which will satisfy the local mass conservation, while the global mass conservation is obtained by solving equation (9).

4 Model validation

The newly developed model has been validated by testing a standing wave in a closed basin of square domain (10 m × 10 m) with the inviscid flow approximation. By choosing a relatively small wave length λ compared to the depth h_0, the hydrostatic approximation is no longer valid. Initially, all velocities are set to zero and the water surface elevation

$$H(x) = \eta_0 \cos\left(\frac{2\pi}{\lambda}x\right) + h_0 \quad \text{with} \quad 0 \le x \le 10\,, \tag{19}$$

where: $\eta_0 = 0.1\,\text{m}$ is the amplitude; $\lambda = 20\,\text{m}$ is the wave length; and $h_0 = 10\,\text{m}$ is the undisturbed water depth. A zero flow Neumann condition is

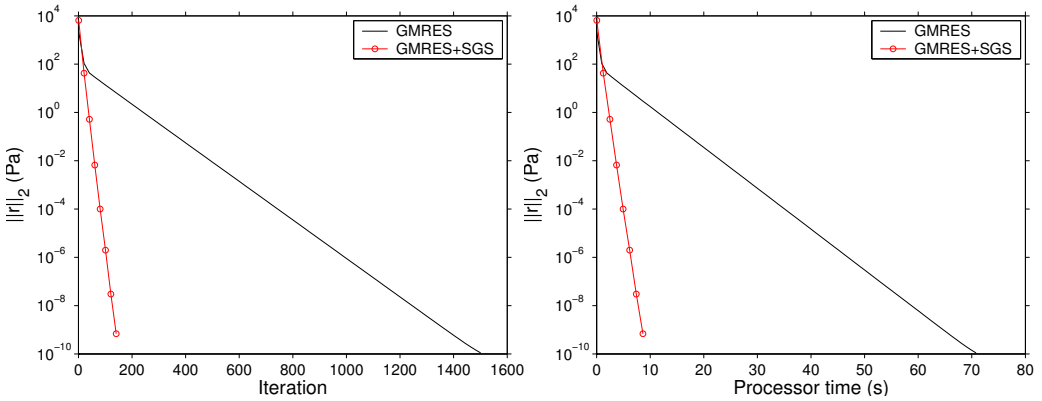

(a) iteration versus residual

(b) processor time versus residual

FIGURE 2: Convergence test for the Poisson equation using the generalised minimal residual (GMRES) method with and without symmetrical Gauss–Seidel (SGS) preconditioning.

used for all three velocities at the wall boundaries, while a free slip condition is applied at the free surface. The computational domain uses a constant grid spacing of 0.5 m in the longitudinal and lateral directions with 20 layers in the vertical direction in order to accommodate the (moving) free surface. Thus, although a rectangular grid is used in the horizontal direction, the vertical grid is adjusted as a result of free surface movements. The time step $\Delta\tau = 0.01\,\mathrm{s}$ is used for all computations.

Based on small amplitude theory [3], the non-hydrostatic pressure wave celerity c is approximated by

$$c = \sqrt{\frac{g\lambda}{2\pi}\tanh\left(\frac{2\pi}{\lambda}h_0\right)}\,, \tag{20}$$

which is equivalent to $c = 5.57\,\mathrm{m/s}$ so that the period T is 3.59 s. Using the

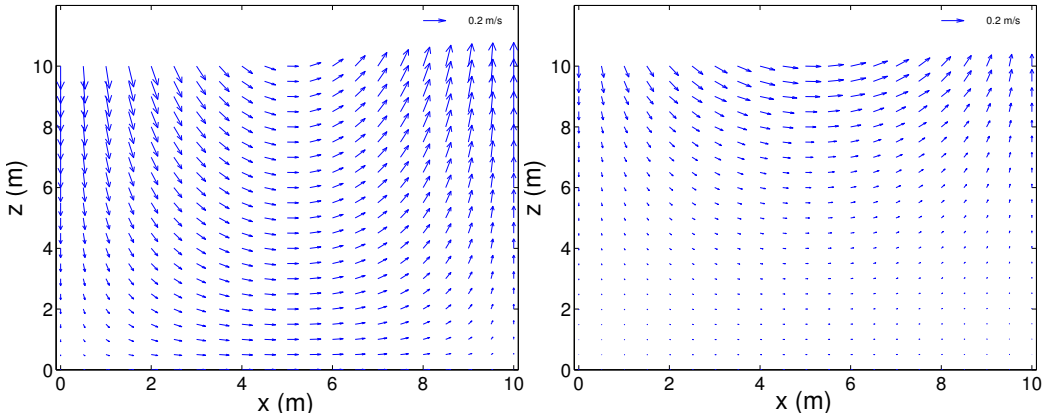

(a) hydrostatic pressure (b) non-hydrostatic pressure

FIGURE 3: Velocity vectors, along the domain centre line $y = 5\,\mathrm{m}$ at time $t = T/4$, with and without the hydrostatic pressure approximation.

hydrostatic pressure approximation, on the other hand, the wave celerity is given by $c = \sqrt{gh_0} = 9.90\,\mathrm{m/s}$, and $T = 2.02\,\mathrm{s}$. Therefore the sloshing wave of the hydrostatic model will propagate at a faster speed than that of the non-hydrostatic model.

Let us examine the convergence rate of the Poisson equation using the GMRES method with and without SGS preconditioning. In Figure 2, the y axis represents the Euclidean norm of the residual, $r = b - Ax^{(m)}$, plotted against the number of iterations in Figure 2(a) and the processor time in Figure 2(b). As expected, the GMRES method with SGS preconditioning reduces both the number of iterations and processor time dramatically even though extra calculations are needed for the preconditioning.

Figure 3 shows the velocity fields along the domain centre line $y = 5\,\mathrm{m}$ at time $t = T/4$, calculated with and without the hydrostatic pressure ap-

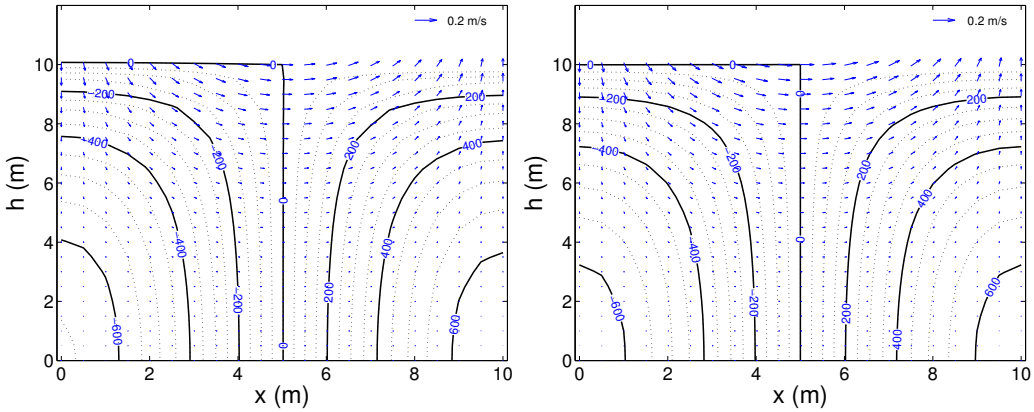

(a) computed (b) analytical

FIGURE 4: Velocity (vectors) and hydrodynamic pressure fields (lines), along the domain centre line $y = 5\,\mathrm{m}$ at time $t = T/8$, as computed by the model and as determined analytically.

proximation, which is equivalent to $t = 0.505\,\mathrm{s}$ and $t = 0.898\,\mathrm{s}$, respectively. The most significant difference is that the hydrostatic model calculates much larger vertical velocities near the walls than the non-hydrostatic model. This is because, with the hydrostatic approximation, these velocities are calculated by solving the continuity equation so that they are only a function of the horizontal velocity field. The results from the hydrostatic model suggest that velocity variations over depth, especially near $x = 5\,\mathrm{m}$, are almost negligible; this is consistent with the shallow water approximation.

Analytic solutions to this free surface problem have been developed using small amplitude theory [3]. In Figure 4 the computed velocity and hydrodynamic pressure fields are compared, along the domain centre line $y = 5\,\mathrm{m}$ at time $t = T/8$, with the analytical solutions. At this time, the water surface is dropping to the equilibrium position on the left and rising

on the right; negative pressure is shown on the left hand side. Excellent agreement between these results indicates that the normal velocity boundary condition has been applied to the pressure-Poisson equation correctly. More computational results of velocity vectors and non-hydrostatic pressure fields for one wave period of this simulation are available as a movie file at http://anziamj.austms.org.au/V46/CTAC2004/Lee1/standing.mov.

5 Conclusion

In this paper, a 3D numerical model with and without the hydrostatic approximation is presented using a generalised coordinate system. Time integration is performed using two fractional time steps. In the hydrostatic step, the intermediate velocity field is solved using a Newton–GMRES method. By considering the non-hydrostatic pressure and the continuity equation, the intermediate velocities are updated to the divergence free velocities in the non-hydrostatic step. In the second step, the pressure-Poisson equation is solved using the GMRES method with SGS preconditioning. The application of this preconditioning to free surface flows indicates significant improvement in convergence and processor time. The new model has been tested with an idealised case, and compared with analytical solutions. Overall agreement with the analytical solutions verifies the accuracy of the new numerical model. In addition, a detailed presentation of the results in movie form shows the advantages of using this new model.

References

[1] P. N. Brown and Y. Saad. Hybrid Krylov methods for nonlinear systems of equations. *SIAM J. Sci. Stat. Comput.* 1990, **11**:450–481. C629

[2] V. Casulli. A semi-implicit finite difference method for non-hydrostatic, free-surface flows. *Int. J. Numer. Meth. Fluids* 1999, **30**:425–440. URL C625, C626

[3] R. G. Dean and R. A. Dalrymple. *Water Wave Mechanics for Engineers and Scientists.* World Scientific, 1991. C631, C633

[4] K. A. Hoffmann and S. T. Chiang. *Computational Fluid Dynamics for Engineering: Volume II.* Engineering Education System, 1993. C626

[5] W. Huang and M. Spaulding. 3D model of estuarine circulation and water quality induced by surface discharges. *J. Hydraul. Eng.* 1995, **121**:300–311. URL C624, C625

[6] M. B. Koçyigit, R. A. Falconer and B. Lin. Three-dimensional numerical modelling of free surface flows with non-hydrostatic pressure. *Int. J. Numer. Meth. Fluids* 2002, **40**:1145–1162. http://dx.doi.org/10.1002/fld.376. C625

[7] Q. Lu and O. W. H. Wai. An efficient operator splitting scheme for three-dimensional hydrodynamic computations. *Int. J. Numer. Meth. Fluids* 1998, **26**:771–789. URL C624, C625

[8] S. V. Patankar. *Numerical Heat Transfer and Fluid Flow.* McGraw Hill, 1980. C625, C627

[9] Y. Saad. *Numerical Methods for Large Eigenvalue Problems (Algorithms and Architectures for Advanced Scientific Computing).* John Wiley and Sons Inc, 1992. C630

[10] G. Stelling and M. Zijlema. An accurate and efficient finite-difference algorithm for non-hydrostatic free-surface flow with application to wave propagation. *Int. J. Numer. Meth. Fluids* 2003, **43**:1–23. http://dx.doi.org/10.1002/fld.595. C625

[11] H. C. Yee. Construction of explicit and implicit symmetric TVD schemes and their applications. *J. Comput. Physics* 1987, **68**:151–179. http://dx.doi.org/10.1016/0021-9991(87)90049-0. C628